Planetary boundary layer height from CALIOP compared to radiosonde over China

Wanchun Zhang[1], Jianping Guo[1], Yucong Miao[1,2], Huan Liu[1], Yong Zhang[3], Zhengqiang Li[4], Panmao Zhai[1]

[1]State Key Laboratory of Severe Weather, Chinese Academy of Meteorological Sciences, Beijing 100081, China
[2]Department of Atmospheric and Oceanic Sciences, Peking University, Beijing 100871, China
[3]Meteorological Observation Centre, China Meteorological Administration, Beijing, 100081, China
[4]State Environmental Protection Key Laboratory of Satellites Remote Sensing, Institute of Remote Sensing and Digital Earth of Chinese Academy of Sciences, Beijing 100101, China

Correspondence to: Jianping Guo (jpguocams@gmail.com) and Panmao Zhai (pmzhai@cma.gov.cn)

Abstract. The accurate estimation of planetary boundary layer height (PBLH) is key to air quality prediction, weather forecast and so on. The PBLH retrieval from CALIOP is expected to complement the ground-based site measurement due to its large spatial coverage. To such end, PBLHs are estimated from CALIOP, using the combination of Haar wavelet and maximum variance techniques, which are then validated against PBLHs from ground-based lidar at Beijing and Jinhua. Comparison between PBLHs from ground- and satellite-based lidars leads to a correlation coefficient of 0.59 in Beijing and 0.65 in Jinhua. Also, the PBLH climatology from CALIOP and radiosonde are compiled over China during the period from 2011 to 2014. Maximum CALIOP-derived PBLH can be seen in summer as compared to lower values in other seasons. Three matchup scenarios are proposed according to the position of each radiosonde site relative to its closest CALIPSO ground tracks. For each scenario,

intercomparisons were performed between CALIOP- and radiosonde-derived PBLHs, and Scenario 2 is found to be better, owing to smaller difference between them. In early summer afternoon over 70% of the total radiosonde sites have PBLH values ranging from 1.6 km to 2.0 km. Overall, CALIOP-derived PBLHs seem to be well consistent with radiosonde-derived PBLHs. To our knowledge, this study is the first intercomparison study of PBLH over large scale using the radiosonde network of China, shedding important light on the data quality of initial CALIOP-derived PBLH results.

1. Introduction

The planetary boundary layer (PBL), the lowest layer of troposphere closest to the surface, is directly influenced by the presence of the Earth's surface, and responds to surface forcings (e.g. sensible heat flux, mechanical drag) on a timescale of about an hour or less (Stull, 1988). The terrestrial PBL is extremely complex, given the nonlinearity and complexity of convective and turbulent processes occurred within PBL. The PBL processes play significant roles in modulating the exchange of momentum, heat, moisture, gases, and aerosols between the Earth's surface and the free troposphere (Hu et al., 2010, 2014; Miao et al., 2015). Therefore, a growing consensus has been reached on the role boundary layer processes and its structures have being played in greatly advancing our capabilities in understanding and predicting weather, climate and air quality (Medeiros et al., 2005; Hong et al., 2006; Zhang et al., 2007; Hu et al., 2010).

The PBL height (PBLH), which determines the vertical extent of turbulent mixing and convection activity within it, is a key length scale in weather, climate, and air quality models. The accurate prediction of vertical diffusion, cloud formation, and pollutant deposition in turn relies on the reliable

parameterization of PBL (Hu et al., 2006; Seibert 2000; Xie et al., 2012). The PBLH typically varies from less than one hundred meters to several thousand meters (Hennemuth and Lammert, 2006). The most common PBLHs are derived from radiosonde soundings of temperature, humidity, and so on. The balloons are required to be launched twice daily for the purpose of operational weather forecast, or 4-8 times per day from the perspective of scientific research during intensive observation period (Seibert, 2000; Liu and Liang, 2010). Although the radiosonde can provide height-resolved temperature and humidity profiles for accurate estimation of PBLH, which is independent of cloud cover conditions, it is still too sparse to detect the PBL evolution over large spatial scale, and thus cannot adequately serve the PBL research on global or even regional scales (Sawyer and Li, 2013). With the limited available radiosonde observations (mostly from the Unite States and Europe), Seidel et al. (2010; 2012) constructed a general picture of PBLH climatology on a global scale. However, they did not give much detailed information of PBL over China, in part due to the lack of high-resolution observations in China. In 2011, a land-based radiosonde network across China has been successfully deployed by the China Meteorological Administration (CMA), which provides a unique opportunity to fill in the gap left.

In addition to the land-based radiosone observations, the lidars that allow the measurement of aerosol or trace gas profiles can be used to study PBL structure (Seibert, 2000). It is well known that aerosol concentrations vary significantly with height, which not only affects the detection of boundary layer, but also may be a large source of uncertainty particularly for satellite-based aerosol retrievals using wavelength of ultraviolet (UV) (e.g., Torres et al., 1998, 2013; Huang et al., 2015). Turning to the measurements of active remote sensing instruments, such as Cloud Aerosol LIdar with Orthogonal Polarization (CALIOP) aboard Cloud-Aerosol Lidar and Infrared Pathfinder Satellite Observations (CALIPSO) (Winker et al., 2007), aerosols can be detected and used as tracers of PBL dynamics. This

is most likely due to the fact that the number of aerosol particles in the PBL is often greater than that in the free troposphere (Leventidou et al., 2013). More importantly, unlike the radiosonde measurement that only provides a "snapshot" of PBL profile at a fixed site (Seibert et al., 2010), the spaceborne lidar can obtain PBL variation over large area of interest, especially over remote regions (Jordan et al., 2010; Zhang et al., 2015).

The overpass time of CALIOP/CALIPSO is around 1330 Local Time (LT), which is almost coincident with the atmospheric sounding observations around 1400 Beijing Time (BJT) operated by CMA in the summer. In the late morning and afternoon time, when the convective boundary layer is well established, strong gradient of aerosol particles can often be seen at the top of convective boundary layer, and thus the lidar-detected PBLH is generally in good agreement with the radiosonde-derived PBLH (Garratt, 1994; Seibert, 2000; Hennemuth and Lammert, 2006). Therefore, at the time of CALIOP overpasses (1330 LT), it seems suitable for determining the convective boundary layer height.

As one of the first attempts to validate the CALIOP-derived PBLHs, Kim et al. (2008) carried out the intercomparison studies between PBLHs from radiosondes and CALIOP measurements, showing high consistence between them. Among others, Ho et al. (2015) compared the marine boundary layer heights from CALIOP profiles with those from radiosonde soundings. On the other hand, large biases of the seasonal and diurnal variations in PBLHs were observed, most likely due to the different methods utilized to radiosonde, ground-based lidar, CALIOP observations over one site in South Africa (Korhonen et al., 2014). Although CALIOP possesses the ability to derive PBLHs over large and remote regions on a regular basis, these comparison studies only involved one or a few sites, and a comprehensive evaluation of CALIOP-derived PBLH with large scale land-based radiosonde

observations remains lacking. In this study, the long-term CALIOP-derived PBLH over China will be validated and assessed by means of the measurements of land-based radiosonde network of CMA.

From the climatological point of view, the PBLH retrieval from CALIOP is expected to complement the ground-based site measurement due to its large spatial coverage. The main objective of this study is twofold: (1) to construct a climatological CALIOP-derived PBLH dataset; (2) to quantify the discrepancies between CALIOP-derived and radiasonde-derived PBLHs. The remainder of this paper proceeds as follows: the data and methods used are described in Section 2. Section 3 reports the comparison results of CALIOP-derived PBLH using ground-based lidar measurements. The spatial and temporal distribution pattern of CALIOP-derived PBLH is presented as well. Moreover, intercomparisons between PBLHs derived from CALIOP and radiosonde measurements will be performed. Last, a brief summary is given in Section 4.

2. Data and methods

2.1 Radiosonde observations and their processing

The radiosonde measures once per second, acquiring detailed vertical profiles of temperature, pressure, relative humidity, wind speed and wind direction over a given weather station. The sounding balloons are operationally launched twice a day at fixed time, i.e. 0800 BJT and 2000 BJT, throughout all the radiosonde sites shown in Figure 1. Fortunately, CMA required the soundings to be launched three to four times a day in summer (the wet season), i.e., 0200 BJT, 0800 BJT, 1400 BJT, and 2000 BJT to seamless monitor the vertical structure of atmosphere, and thus to better serve the high-impact

weather forecasting. Owing to our focus on the convective PBL in the daytime, the 1400 BJT soundings in summer allow us to determine PBLHs over most weather sites throughout China, which are used for comparison analysis with CALIOP-derived PBLH being typically available at 1330 LT.

As summarized in Seidel et al. (2010), there are seven commonly used methods to derive PBLHs based on the profiles of temperature, potential temperature, virtual potential temperature, relative humidity, specific humidity, and refractivity. The traditional approach encountered in the textbooks (e.g., Oke, 1988; Sorbjan, 1989; Garratt, 1992) typically defines PBLH as the pressure level where the maximum vertical gradient of potential temperature occurs, indicative of a transition from a convectively less stable region below to a more stable region above. Recently, a more sophisticated method (Brooks, 2003; Davis et al., 2000) involves the wavelet covariance transform. In contrast, the algorithm of wavelet covariance transform was first proposed by Gamage and Hagelberg (1993) as a way to detect step changes in a signal.

By combining the methods of wavelet covariance and iterative curve-fitting (Steyn et al., 2009), Sawyer and Li (2013) developed a novel algorithm (hereafter called SL2013), which can be applied to robustly derive PBLHs from both radiosonde and lidar measurements due to the fact that prior knowledge of instrument properties and atmospheric conditions has been adequately considered. The measurement time of our study is almost at noon, the potential temperature profile more often than not exhibit the typical structure of convective BL. However, due to the potential uncertainties caused by the sensitivity of vertical resolution, and the wide range of sounding time (in LT) at different sites across China, SL2013 tends to exhibit advantages over the method of maximum potential temperature gradient. This is most likely because SL2013 is flexible and simple enough for automatic analyses of long-term sounding data at multiple sites, and is able to compensate for noisy signals and low vertical resolution in

the soundings. Therefore, SL2013 has been applied to extract PBLHs from radiosonde observations. However, bear in mind that the extreme adverse weather, which is also an important influential factor, will inevitably exert large uncertainties on the retrieved PBLH. For instance, the PBL as deep convective cloud occurs will collapse, leading to an extremely large value. These cases will be excluded for further comparison analysis with CALIOP-derived PBLHs. The sounding observations of 113 radiosonde sites (black dots in Figure 1) during the period 2011-2014 are then used to calculate PBLHs, and perform comparison analysis with the CALIOP-derived PBLHs as well.

2.2 Ground-based lidar observations

Ground-based lidar observations from two sites (i.e., Beijing and Jinhua) have been used to evaluate the PBLHs retrieved from CALIOP. The site of Beijing (40.00°N, 116.38°E) is located on the campus of the Institute of Remote Sensing and Digital Earth, Chinese Academy of Sciences, where the CE370 micro-pulse Lidar (made by CIMEL of France) was deployed during the period of January 1, 2014 to December 31, 2014. The profiles of aerosol backscatter coefficient obtained from CE370 have a vertical resolution of 15 m. The laser transmitter system is reported to have a diameter of 20cm, which is used to expand laser beam through a refracting telescope.

The other ground-based lidar was deployed on the campus of Zhejiang Normal University of Jinhua (29.0°N, 119.5°E), Zhejiang Province. The altitude of this site is 71m above sea level. Jinhua, located in the Yangtze River Delta of East China, underwent increasingly polluted air quality due to the rapid economic development in recent years (Guo et al., 2011; Wang et al., 2015). The ground-based lidar deployed at Jinhua are similar to CALIOP with two orthogonally polarized channels at 532 nm and one

channel at 1064 nm. The algorithm developed by Zhang et al. (2015) has been applied to the profiles of ground-based lidars deployed at Beijing and Jinhua, respectively. To be more specific, only the segment of CALIOP profiles within a circle of 75km radius centered at the abovementioned two ground-based lidar sites are included in the PBLH retrievals. Due to the neighbouring ground tracks of CALIPSO at approximately 100-150 km longitudinal interval over China, a 75km-radius circle centered at each ground-based lidar site has been determined for its matchup with CALIOP, so has the matchup of radiosonde site with CALIOP.

The lidar has been shut off (1) during midday in summer to prevent the optics from harms caused by intense sunlight, (2) during maintenance period of lidar, or (3) during the time period when lidar cannot normally work, leading to unwanted breaks of lidar observations. Meanwhile, unfavorable weather conditions, including rains, heavy haze episodes, among others, generally lead to unreliable PBLH retrievals. Overall, the data volume fraction is roughly 87.7 % for Beijing site. The lidar measurements with PBLH detection differ largely by month. A total of 133 hours are obtained in May, as compared with 661 hours in March (Figure S1). Given the unreliable PBLH retrievals under some unfavourable conditions as described above, the annual average of the data is reduced to 64%, similar to 72% over Jinhua site.

2.3 CALIOP observations and their processing

The CALIOP onboard the CALIPSO platform (flying as part of the A-Train satellite constellation since April 2006) is a three-channel elastic backscatter lidar, which is optimized for aerosol and cloud profiling. It measures attenuated backscatter coefficients at a resolution of 1/3 km in the horizontal at

the visible wavelength (532 nm) and near-infrared wavelength (1064 nm), and its vertical resolution varies with altitude (h): 30m from ground up to h = 8.2 km, 60m from h = 8.2 km to 20.2 km, and 180m from h = 20.2 km to 30.1 km (Winker et al., 2009; Huang et al., 2015). All satellites of the A-train constellation are in a 705-km sun-synchronous polar orbit between 82 °N and 82 °S with a 16-day repetition cycle, with a nominal ascending node equatorial crossing time of 1330 (0130) local day (night) time (Liu et al., 2009; Winker et al., 2007; Winker et al., 2003). As shown in Figure 1, red lines represent the ground tracks over China for the daytime overpasses of CALIPSO (in ascending mode), while blue lines ground tracks for nighttime overpasses of CALIPSO (in descending mode). The neighboring ground track is at a longitudinal interval of approximately 150-km, varying with latitudes.

The PBLH is predominantly estimated from the CALIOP Level 1 product: the total attenuated backscatter coefficient, in combination with Level 2 product of cloud layer products (1/3 km in the horizontal) for cloud screening. Resembling the methods utilized to derive PBLHs proposed by Jordan et al. (2010), we rely on the maximum variance algorithm to derive PBLHs from CALIOP attenuated backscatter coefficient profiles at wavelength of 532 nm, in combination with the Haar wavelet technique. The maximum variance algorithm is originated from the ideas proposed by Melfi et al. (1985) and heavily relies on the existence of a strong aerosols concentration gradient at the top of the PBL, which corresponds to the levels where the maximum standard deviation occurs of lidar backscatter. This method has been widely used to derive PBLHs from CALIOP so that the global seasonal variations can be inferred (McGrath-Spangler and Denning, 2012, 2013). However, either maximum variance algorithm or Haar wavelet technique has its weakness due to the strong dependence on the chosen strategy in the threshold values. To make the comparison of radiosonde-derived PBLHs with CALIOP-derived PBLHs more reliable and robust, the combined algorithm has been applied on the

corresponding profiles of CALIOP according to the matchup scheme described in section 2.2. All the comparisons are limited to daytime measurements due to the nature of convective boundary layer, unless noted otherwise.

Due to the most likely blocking and attenuation caused by optically thin or thick clouds, we have to perform the cloud-screen procedures prior to the algorithm mentioned above operating on the CALIPSO level 1 profile data. The CALIPSO measurements were retained for PBLH retrievals at grid points where the number of valid (i.e., without cloud) CALIPSO overpasses exceeded 15% of the total number of overpasses. As such, we can minimize the effect of clouds on the retrieved PBLHs to a certain degree. Meanwhile, to improve the signal-to-noise ratio (SNR) for better PBLH retrievals, roughly 15 CALIOP profiles with 333-m resolution along track have to be resampled to one 5-km resolution profile for all CALIOP observations.

As a good case in point for a better view of the results derived using the above algorithms, the CALIOP-derived PBLHs (indicated by the black line) on 15 January 2011 over southeastern China is shown in Figure 2. By visual interpretation, we can see that the derived-PBL tops are just located at the levels where aerosol backscatter signals change abruptly.

3. Results and discussion

3.1 Comparison of CALIOP-derived PBLH against ground-based lidar-derived PBLH

In order to make the intercomparison more reliable between CALIOP- and radiosonde-derived PBLHs, the former has to undergo an evaluation using ground-based lidar, which typically shares the similar techniques. To minimize the influence of cloud on the PBLH determination from lidar, all the

lidar measurements of Beijing and Jinhua with clouds (extracted directly from the meteorological data at neighbouring weather station) have been excluded for further analyses.

The scatter plots are shown in Figure 3 concerning the intercomparison between the ground-based lidar derived PBLHs and CALIOP-derived PBLHS over Jinhua and Beijing (40.0°N, 116.4°E). Due to the twice-per-month revisit period of CALIPSO satellite, only 17 cases out of 24 at Beijing are selected, in which both CALIOP and ground-based lidar have simultaneous measurements at 1330 LT. And the simultaneous PBLH retrievals have been carried out for 7 cases out of 12 at Jinhua. For the overall comparison between the PBLHs derived from ground-based lidar and CALIOP, the correlation coefficient through orthogonal regression reaches 0.59 at Beijing and 0.65 at Jinhua, respectively. Due to the samples being still limited, so we cannot be quite sure to argue that the CALIOP-derived PBLHs are reliable enough. Further evaluation studies are warranted in the future as long as more ground-based lidar observations are available. However, the correlation coefficients obtained here are similar to those reported at SACOL site of northwestern China (e.g., Liu et al., 2015).

3.2 CALIOP-derived PBLH Climatology throughout China

Figure 4 presents the spatial distributions of seasonal mean PBLHs with $0.2^o \times 0.2^o$ resolution derived from CALIPSO afternoon measurements during the period 2011 through 2014. The original 5 km PBLH data have been smoothed and resampled to 20 km resolution to highlight the coherent large-scale structures. It can be clearly seen that the PBLHs over China exhibit large spatial and seasonal variations. On average, both Figure 4 and Table 1 indicate that the highest PBLHs ($1.82\text{km} \pm 0.31\text{km}$) were seen in summer (June, July and August), mainly ranging from 1.5 to 2.5 km. On the other hand, the lowest

PBLH values (1.51km ± 0.40km) occur in winter (December, January and February) when the development of PBL is typically suppressed due to the less solar radiation received at the surface. In contrast, the more intense solar radiation reaching the surface in summer favours the development of PBL (Stull et al., 1988). As shown in Table 1, we notice that the maximum PBLHs can reach up to 5-6 km, especially in winter. Therefore, we set the CALIOP-retrieved PBLHs to be within 0.25 and 3km, which seems as a reasonable height range for the midday PBL, highly consistent with the processing methods by McGrath-Spangler (2012). Statistics showed that only 2.1% of all data higher than 3km and 8.8% lower than 0.25km, which have been excluded for further analyses.

In terms of the discrepancy in spatial distribution of PBLH, the Tibetan Plateau (TP) was characterized by high values, irrespective of the evolution of seasons. Over eastern China, particularly the regions with large population and severe air pollution (Guo et al., 2009; 2011) (e.g. North China Plain, the Yangtze River Delta, and Pearl River Delta), the PBLHs were higher in spring and summer, but did not show expected large seasonal variation. During the seasons (such as winter) when haze event frequently occurs, due to the suppression by aerosol radiative effects and aerosol-wind interactions (Xia et al., 2007; Yang et al., 2016), relatively shallow PBLHs can be apparently seen across most of China, in good agreement with previous findings (e.g., Quan et al., 2013; 6Gao et al. 2015; Miao et al, 2016). This aerosol-rich haze, in combination with lowered PBL, tends to significantly delay the precipitation and its peak (Guo et al., 2016). The spatial distribution of PBLH revealed a tendency for higher PBLH over high elevation regions, consistent with dependence on elevation reported in the United States (Seidel et al., 2012). Such spatial variation of PBLH may be related to the local land surface and hydrological processes (Seidel et al., 2012).

3.3 Matchup between CALIOP profiles and radiosonde soundings

As revealed in Section 2.3, we have averaged out the PBLHs derived from the CALIOP profiles, which are then involved in comparison analysis with the mean PBLHs from radiosonde soundings. After multiple rounds of iteration through the positions of each radiosonde site over China relative to its closest CALIPSO ground tracks, a total of three scenarios are representative of all the cases, as shown in Figure 5. Scenario 1 denotes the cases with two CALIOP ground tracks, the shortest distance to which each is more than 37.5km from each radiosonde site. In contrast, Scenario 2 represents the cases with one CALIOP ground track, the shortest distance to which is less than 37.5km from each radiosonde site. Scenario 3 is the same as Scenario 2 except for the shortest distance to which is more than 37.5km from radiosonde site.

The details of classification criteria are summarized in Table 2. Out of the total of 113 radiosonde sites were classified, 64 sites belonged to Scenario 2. That means about 56.6% of all radiosonde sites make a good match with CALIOP profiles for its nearest distance to CALIPSO ground tracks less than 37.5km. By comparison, there are 22 sites (19.5%) attributed to Scenario 1 whereas 27 sites (23.9%) scenario 3.

Figure 6 shows the geographic distribution concerning the location of radiosonde sites relative to its closest CALIOP ground tracks inside a circle of radius 75 km over China, which are stratified by Scenarios 1, 2, and 3. Owing to the nearest distance to radiosonde site in Scenario 2, profiles in CALIOP observations can be used to better capture the PBL evolution, and thus facilitate the intercomparisons. It happens that the radiosonde sites (56.6%) belonging to Scenarios 2 are uniformly distributed over China, indicating that most of the radiosonde sites in China can be collocated well with afternoon CALIPSO overpass.

Interestingly, the radiosonde sites for Scenario 1 are mostly located in the northern China, as opposed to those for Scenarios 3 in the southern China. The more northward the radiosonde sites, the greater

number of the CALIPSO overpasses over the same circle of 75 km radius. Therefore, the distinct discrepancy in geographic distributions of radiosonde sites belonging to Scenarios 1 and 3 are most likely due to the latitude differences. More importantly, because the region of interest (China) spans several time zones, the spatial variations of radiosonde-derived PBLHs observed at fixed observation times (1400 BJT) tend to be conflated with diurnal variations, as discussed in the following Section 4.

3.4 Intercomparison between CALIOP- and radiosonde-derived PBLHs

Using the algorithms as detailed in Section 2, the PBLHs at all the 113 radiosonde sites have been successfully derived from radiosonde and CALIOP. In terms of the spatial differences of PBLHs, both CALIOP retrievals (Figure 4b) and radiosonde observations (Figure S2) show that large PBLH values tend to occur at Tibetan Plateau, southwestern China, and northern China in early summer afternoon. This is likely indicative of good agreement between CALIOP- and radiosonde-derived PBLH retrievals. Furthermore, the differences of PBLHs at every radiosonde sites (Figure 1) from CALIOP measurements at 1330 LT minus those from radiosonde observations at 1400 BJT in the summertime (June-July-August) during the period of 2011-2014 are calculated. In the mean time, the differences of PBLHs have to be averaged out for each radiosonde sites again according to three matchup scenarios for both CALIOP profiles and radiosonde sites described in Table 2.

As shown in Figure 7(a), the PBLH differences over most of the radiosonde sites to the east of 110 ^{o}E longitude exhibit negative values, indicating CALIOP-derived PBLHs tend to be underestimated compared with radiosonde-derived PBLHs. In contrast, it is a different story (to be overestimated as compared with radiosonde) for the sites to the west of 110 ^{o}E longitude (the western China), especially in provinces such as Xinjiang, Sichuan and Chongqing. The CALIOP observations at roughly 1330 LT in the western China has been compared with the radiosonde measurements at 1400 BJT which

corresponds to 1100-1400 LT differing by longitudes, therefore, the relatively low PBLHs from the radiosondes in the west China are expected to be in association with weak convection. This in turn leads to overestimated CALIOP-derived PBLHs in the western China. However, there are other aspects neglected to be discussed here, which are likely to be contributed to the discrepancies between the two data sources.

All sites in Figure 7 (a) are divided into three subgroups according to the matchup scenario described in previous sections. Overall, the radiosonde-derived PBLHs tend to be overestimate compared with CALIOP-derived PBLHs due to the majority of radiosonde sites (77 of 113 sites, i.e., 68%) showing lower PBLH values. This is also consistent with the results shown in Table 2. As shown in Figures 7b-d, the average biases between CALIOP- and radiosonde-derived PBLHs for Scenario 2, as expected, have smaller magnitude (0.17 km), as compared with Scenario 1 (with a magnitude of 0.22 km). On the other hand, the smallest average bias (0.15 km) is observed for Scenario 3. More statistics with regard to the biases between CALIOP- and radiosonde-derived PBLHs are illustrated in Figure 8.

As indicated in Figure 8, Scenario 2 witnesses the least difference of 0.08km between the CALIOP- and radiosonde-median PBLH values in contrast to larger differences of 0.24km and 0.12km for Scenario 1 and Scenario 3, respectively. In addition, the PBLH differences in terms of 25^{th} and 75^{th} percentile values for Scenario 2 are much more indiscernible, as compared with those for other two scenarios. This implies that Scenario 2 gains more advantages over other two scenarios due to the smaller difference between CALIOP- and radiosonde-derived PBLHs.

Figure 9 shows the frequency of occurrence for the number of radiosonde sites, which are stratified by binned radiosonde-derived mean PBLHs (1400 BJT) and CALIOP-derived mean PBLHs (around 1330 LT) over China in the summertime (June-July-August) during the period of 2011-2014. Typically

speaking, the PBLHs in early summer afternoon over China range from 1.6 km to 2.0 km, accounting for over 70% of the total radiosonde sites. The pattern in Figure 9(c) is more similar to that in Figure 9(a), suggesting that the results from Scenario 2 to some extent are representative of the overall results over all sites. In other words, comparison of the histogram of CALIOP PBLHs to the radiosonde observations indicates that they are in good enough agreement with each other.

4. Conclusions

This study presents initial validation results of space-borne CALIOP-derived PBLHs by comparing with coincidental observations from two ground-based lidars at Beijing (from January 1, 2014 to December 31, 2014) and Jinhua (from June 1, 2013 to December 31, 2013). Results show that the correlation coefficient is about 0.59 in Beijing and 0.65 in Jinhua, respectively. The selected data set represents two different underlying land surfaces, i.e., urban and mountain area, both of which are obtained under cloud-free conditions.

The climatology of seasonal mean PBLHs at $0.2^o \times 0.2^o$ resolution has been constructed, as derived from afternoon CALIPSO measurements during the period 2011 through 2014. The PBLHs over China are found to exhibit large spatial and seasonal variations. Overall, summer (June, July and August) tend to have highest PBLH values, as opposed to the lowest PBLH values occurring in winter (December, January and February). Such seasonal variation of PBLH may be caused by the seasonal variation of solar radiation.

Prior to the comparison analysis between CALIOP- and radisonde-derived PBLHs, three matchup scenarios are proposed according to the position of each radiosonde site over China relative to its

closest CALIPSO ground tracks. The matchup of each radiosonde site with its neighbouring CALIPSO ground tracks can be attributed to one the three scenarios. The spatial distribution of radiosonde sites belonging to Scenario 2 indicates that most of the radiosonde sites in China can be collocated very well with afternoon CALIPSO overpass. Further intercomparison analyses suggest that CALIOP observations belonging to Scenario 2 seem to be better as compared with radiosonde-derived PBLH, due to much smaller difference between them.

Overall, CALIOP-derived PBLHs tend to be underestimated compared with radiosonde-derived PBLHs. On the other hand, more than 70% of the radiosonde sites across China in early summer afternoon have relatively higher PBLH values, which vary from 1.6 km to 2.0 km. Therefore, CALIOP PBLHs tend to agree pretty well with radiosonde-derived PBLHs. Despite the limitation in the presence of clouds, CALIOP has been routinely available for determination of PBLHs and therefore is a valuable method for long-term climatology analyses. To our knowledge, this study is the first intercomparison study of PBLHs between CALIOP- and radiosonde-derived PBLHs over large scale using the radiosonde network of China, although much detailed regional analyses have not been dealt with, which merit further investigation in the near future.

Acknowledgements

This study was financially supported by the National Natural Science Foundation of China (Grant 91544217), Ministry of Science and Technology of China (Grant no. 2014BAC16B01), Natural Science Foundation of China (Grant 41471301) and Chinese Academy of Meteorological Sciences (Grant 2014R18). The authors would like to acknowledge CMA for providing the radiosonde dataset for us to

use. Special thanks go to NASA for making the CALIOP products accessible for public use, Anhui Institute of Optics and Fine Mechanics (AIOFM) and Institute of Remote Sensing and Digital Earth of Chinese Academy of Sciences, Chinese Academy of Sciences (CAS) for providing the ground-based lidar data.

Reference

Brooks, I.M.: Finding boundary layer top: Application of a wavelet covariance transform to lidar backscatter profiles. J. Atmos. Oceanic Tech., 20, 1092-1105, 2003.

Davis, K.J., Gamage, N., Hagelberg, C., Kiemle, C., Lenschow, D., Sullivan, P.: An objective method for deriving atmospheric structure from airborne lidar observations. J. Atmos. Oceanic Tech., 17, 1455-1468, 2000.

Gao, Y, Zhang, M, Liu, Z, Wang, L, Wang, P, Xia, X, Tao, M, Zhu, L.: Modeling the feedback between aerosol and meteorological variables in the atmospheric boundary layer during a severe fog–haze event over the North China Plain. Atmos. Chem. Phys., 15(8): 4279–4295, doi: 10.5194/acp-15-4279-2015, 2015.

Gamage, N., Hagelberg, C.: Detection and analysis of microfronts and associated coherent events using localized transforms. J. Atmos. Sci., 50, 750-756, 1993.

Garratt, J. R.: The Atmospheric Boundary Layer, 335 pp., Cambridge Atmospheric and Space Science Series, Cambridge Univ. Press, 1992.

Guo, J.P., Deng, M.J., Lee, S.-S., Wang, F., Li, Z., Zhai, P.M., Liu, H., Lv, W.T., Yao,W., and Li, X.: Delaying precipitation and lightning by air pollution over Pearl River Delta. Part I: observational analyses, J. Geophy. Res.-Atmos., doi: 10.1002/2015JD023257, 2016.

Guo, J.-P., Zhang, X.-Y., Che, H.-Z., Gong, S.L., An, X.Q., Cao, C.X., Guang, J., Zhang, H., Wang, Y.Q., Zhang, X.C., Xue, M., Li, X.W.: Correlation between PM concentrations and aerosol optical

depth in eastern China. Atmos. Environ., 43, 37, 5876-5886, doi:10.1016/j.atmosenv.2009.08.026, 2009.

Guo, J.P., Zhang, X., Wu, Y.R., Zhaxi, Y., Che, H., La, B., Wang, W., and Li, X.,: Spatio-temporal variation trends of satellite-based aerosol optical depth in China during 1980–2008, Atmos. Environ., 45(37),6802-6811, doi: 10.1016/j.atmosenv.2011.03.068, 2011.

Hu, X., Ma, Z., Lin, W., Zhang, H., Hu, J., Wang, Y., Xu, X., Fuentes, J.D., Xue, M., Impact of the Loess Plateau on the atmospheric boundary layer structure and air quality in the North China Plain : A case study. Sci. Total Environ. Elsevier B.V. **499**: 228–237. DOI: 10.1016/j.scitotenv.2014.08.053, 2014.

Hu, X.M., Nielsen-Gammon, J.W., Zhang, F. : Evaluation of three planetary boundary layer schemes in the WRF model. J. Appl. Meteorol.Clim., **49**(9): 1831–1844. DOI: 10.1175/2010JAMC2432.1, 2010.

Huang, J., Guo, J., Wang, F., Liu, Z., Jeong, M.J., Yu, H. and Zhang, Z.: CALIPSO inferred most probable heights of global dust and smoke layers. J. Geophys. Res.-Atmos., 120(10), 5085-5100, 2015.

Hennemuth, B., and Lammert, A.: Determination of the Atmospheric Boundary Layer Height from Radiosonde and Lidar Backscatter. Boundary-Layer Meteorol. 120, 181-200, 2006.

Ho, S.-P., Peng, L., Anthes, R.A., Kuo, Y.-H., Lin, H.-C.: Marine Boundary Layer Heights and Their Longitudinal, Diurnal, and Interseasonal Variability in the Southeastern Pacific Using COSMIC, CALIOP, and Radiosonde Data. J. Clim., 28, 7, 2856-2872, doi:10.1175/jcli-d-14-00238.1, 2015.

Hong, S-Y, Noh, Y., Dudhia, J.: A New Vertical Diffusion Package with an Explicit Treatment of Entrainment Processes. Mon. Weather Rev., 134(9): 2318–2341. DOI: 10.1175/MWR3199.1, 2006.

Jordan, N.S., Hoff, R.M., Bacmeister, J.T.: Validation of Goddard Earth Observing System-version 5 MERRA planetary boundary layer heights using CALIPSO. J. Geophys. Res.-Atmos., 115, doi:10.1029/2009jd013777, 2010.

Kim, S. W., Berthier, S., Raut, J.C., Chazette, P., Dulac, F., and Yoon, S. C.: Validation of aerosol and cloud layer structures from the space-borne lidar CALIOP using a ground-based lidar in Seoul, Korea, Atmos. Chem. Phys., 8(13), 3705-3720, doi:10.5194/acp-8-3705-2008, 2008.

Korhonen, K., Giannakaki, E., Mielonen, T., Pfüller, A., Laakso, L., Vakkari, V., Baars, H., Engelmann, R., Beukes, J.P., Van Zyl, P.G., Ramandh, A., Ntsangwane, L., Josipovic, M., Tiitta, P., Fourie, G., Ngwana, I., Chiloane, K., Komppula, M.: Atmospheric boundary layer top height in South Africa: measurements with lidar and radiosonde compared to three atmospheric models. Atmos. Chem. Phys. 14, 4263-4278, 2014.

Leventidou, E., Zanis, P., Balis, D., Giannakaki, E., Pytharoulis, I., Amiridis, V.: Factors affecting the comparisons of planetary boundary layer height retrievals from CALIPSO, ECMWF and radiosondes over Thessaloniki, Greece. Atmos. Environ., 74, 360-366, 2013.

Liu, J., Huang, J., Chen, B., Zhou, T., Yan, H., Jin, H., Huang, Z., Zhang, B.: Comparisons of PBL heights derived from CALIPSO and ECMWF reanalysis data over China. J. Quant. Spectrosc. Radiat. Transfer, 153, 102-112, 2015.

Liu, S., Liang, X.-Z.: Observed diurnal cycle climatology of planetary boundary layer height. J. Clim., 23, 21, 5790-5809, doi:10.1175/2010jcli3552.1, 2010.

Liu, Z., Vaughan, M., Winker, D., Kittaka, C., Getzewich, B., Kuehn, R., Omar, A., Powell, K., Trepte, C., Hostetler, C.: TheCALIPSOLidar Cloud and Aerosol Discrimination: Version 2 Algorithm and Initial Assessment of Performance. J. Atmos. Oceanic Tech., 26, 1198-1213, 2009.

McGill, M.J., Vaughan, M.A., Trepte, C.R., Hart, W.D., Hlavka, D.L., Winker, D.M., Kuehn, R.: Airborne validation of spatial properties measured by the CALIPSO lidar. J. Geophys. Res.-Atmos., 112 (D20), doi: 10.1029/2007JD008768, 2007.

McGrath-Spangler, E.L., Denning, A.S.: Estimates of North American summertime planetary boundary layer depths derived from space-borne lidar. J. Geophys. Res.-Atmos., 117 (D15), doi: 10.1029/2012JD017615, 2012.

McGrath-Spangler, E.L., Denning, A.S.: Global seasonal variations of midday planetary boundary layer depth from CALIPSO space-borne LIDAR. J. Geophys. Res.-Atmos., 118, 1226-1233, 2013.

Medeiros, B., Hall, A., Stevens, B.: What controls the mean depth of the PBL? J. Clim., 18, 3157-3172, 2005.

Melfi, S., Spinhirne, J., Chou, S., Palm, S.: Lidar observations of vertically organized convection in the planetary boundary layer over the ocean. J. Appl. Meteorol. Clim., 24, 806-821, 1985.

Miao Y, Hu X-M, Liu S, Qian T, Xue M, Zheng Y, Wang S.: Seasonal variation of local atmospheric circulations and boundary layer structure in the Beijing-Tianjin-Hebei region and implications for air quality. J. Adv. Model. Earth Sy., **7**(1): 1–25, doi: 10.1002/2015MS000522, 2015.

Miao, Y., Liu, S., Zheng, Y., Wang, S.: Modeling the feedback between aerosol and boundary layer processes: a case study in Beijing, China. Environ. Sci. Pollut. Res., 23(4): 3342–3357, doi: 10.1007/s11356-015-5562-8, 2016.

Oke, T. R.: Boundary Layer Climates, 2nd ed., 435 pp., Halsted Press, New York, 1988.

Quan, J., Gao, Y., Zhang, Q., Tie, X., Cao, J., Han, S., Meng, J., Chen, P., Zhao, D: Evolution of planetary boundary layer under different weather conditions, and its impact on aerosol concentrations. Particuology. 11(1): 34–40, doi: 10.1016/j.partic.2012.04.005, 2013.

Sawyer, V., Li, Z.: Detection, variations and intercomparison of the planetary boundary layer depth from radiosonde, lidar and infrared spectrometer. Atmos. Environ., 79, 518-528, 2013.

Seibert, P.: Review and intercomparison of operational methods for the determination of the mixing height. Atmos. Environ., 34, 1001-1027, 2000.

Seidel, D.J., Ao, C.O., Li, K., Estimating climatological planetary boundary layer heights from radiosonde observations: Comparison of methods and uncertainty analysis. J. Geophys. Res.-Atmos. 115, 2010.

Seidel, D. J., Zhang, Y., Beljaars, A., Golaz, J.-C., Jacobson, A. R., and Medeiros, B.: Climatology of the planetary boundary layer over the continental United States and Europe.J. Geophys. Res.-Atmos.,117, D17106, doi:10.1029/2012JD018143, 2012.

Sorbjan, Z.:Structure of the Atmospheric Boundary Layer, 317 pp., Prentice Hall, Englewood Cliffs,

N.J., 1989.

Steyn, D.G., Baldi, M., Hoff, R.M.: The detection of mixed layer depth and entrainment zone thickness from lidar backscatter profiles. J. Atmos. Oceanic Tech., 16, 953-959, 1999.

Stull, R.B.: An introduction to boundary layer meteorology. Springer Science & Business Media, 1988.

Torres, O., Ahn, C., and Chen, Z.: Improvements to the OMI near UV Aerosol Algorithm using A-train CALIOP and AIRS observations. Atmos. Meas. Tech., **6**, 5621.5652, doi:10.5194/amtd-6-5621-2013, 2013.

Torres, O., Bhartia, P.K., Herman, J.R., Ahmad, Z., and Gleason, J.: Derivation of aerosol properties from satellite measurements of backscattered ultraviolet radiation: Theoretical basis. J. Geophys. Res.-Atmos., 103**(**D14**)**: 17099-17110, 1998.

Wang, F., Guo, J., Zhang, J., Huang, J., Min, M., Chen, T., Liu, H., Deng, M., Li, X.: Multi-sensor quantification of aerosol-induced variability in warm cloud properties over eastern China, Atmos. Environ., 113, 1-9.doi:10.1016/j.atmosenv.2015.04.063, 2015.

Winker, D.M., Hunt, W.H., McGill, M.J.: Initial performance assessment of CALIOP. Geophys. Res. Lett. 34(19), L19803, doi: 10.1029/2007GL030135, 2007.

Winker, D.M., Pelon, J.R., McCormick, M.P.: The CALIPSO mission: Spaceborne lidar for observation of aerosols and clouds, Third International Asia-Pacific Environmental Remote Sensing Remote Sensing of the Atmosphere, Ocean, Environment, and Space. International Society for Optics and Photonics, 1-11, 2003.

Winker, D.M., Vaughan, M.A., Omar, A., Hu, Y., Powell, K.A., Liu, Z., Hunt, W.H., Young, S.A.: Overview of the CALIPSO Mission and CALIOP Data Processing Algorithms. J. Atmos. Oceanic Tech., 26, 2310-2323, 2009.

Xia, X., Li, Z., Wang, P., Chen, H., Cribb, M.: Estimation of aerosol effects on surface irradiance based on measurements and radiative transfer model simulations in northern China. J. Geophys. Res.-Atmos., 112(22): 1–11, doi: 10.1029/2006JD008337, 2007.

Xie, B., Fung, J.C.H., Chan, A., Lau A.: Evaluation of nonlocal and local planetary boundary layer schemes in the WRF model. J. Geophys. Res.-Atmos., **117**(12): 1–26, doi: 10.1029/2011JD017080, 2012.

Yang, X., Zhao C., Guo J., Wang Y.: intensification of air pollution associated with its feedback with surface solar radiation and winds in Beijing. J. Geophys. Res.-Atmos., 121(8): 4093–4099, doi: 10.1002/2015JD024645, 2016.

Zhang,F., Bei, N., Nielsen-Gammon, J.W., Li, G., Zhang, R., Stuart, A., and Aksoy, A.: Impacts of meteorological uncertainties on ozone pollution predictability estimated through meteo- rological and photochemical ensemble forecasts. J. Geophys. Res.-Atmos., 112, D04304, doi:10.1029/2006JD007429, 2007.

Zhang, W., Augustin, M., Zhang, Y., Li, Z., Xu, H., Liu, D., Wang, Z., Zhang, Y., Ma, Y., Zhang, F.: Spatial and Temporal Variability of Aerosol Vertical Distribution Based on Lidar Observations: A Haze Case Study over Jinhua Basin. Adv. Meteorol., doi: 10.1155/2015/349592, 2015.

Table list:

Table 1. Statistics of the CALIOP-derived PBLH in different seasons during the period 2011 - 2014. The mean PBLHs for all the grids are firstly calculated in China, then the maximum and minimum values of PBLHs are determined by sorting all the mean values. Meanwhile, the mean and standard deviation values of PBLH are determined as the average of mean values at every grid in China.

	Spring	**Summer**	**Autumn**	**Winter**
Maximum PBLH (km)	4.57	4.40	3.60	6.13
Minimum PBLH (km)	0.15	0.38	0.22	0.21
Mean PBLH (km)	1.72	1.82	1.56	1.51
Standard deviation of PBLH (km)	0.35	0.31	0.30	0.40

Table 2. Detailed descriptions with regard to the classification criteria of scenario of the positions of radiosonde site relative to the closest CALIOP profiles, including the number of CALIPSO ground tracks for each scenario, the shortest distance (SD) to ground tracks, the total number of sites for each scenario in China, as well as the number of sites with overestimated averaged PBLHs (OE) or underestimated averaged PBLHs (UE) from CALIOP compared with radiosonde.

Scenario	**# of CALIPSO ground tracks**	**SD** (km)	**# of sites**	**# of sites with OE**	**# of sites with UE**
1	2	37.5<D≤75	22	11	11
2	1	0≤D≤37.5	64	18	46
3	1	37.5<D≤75	27	7	20

Figure list

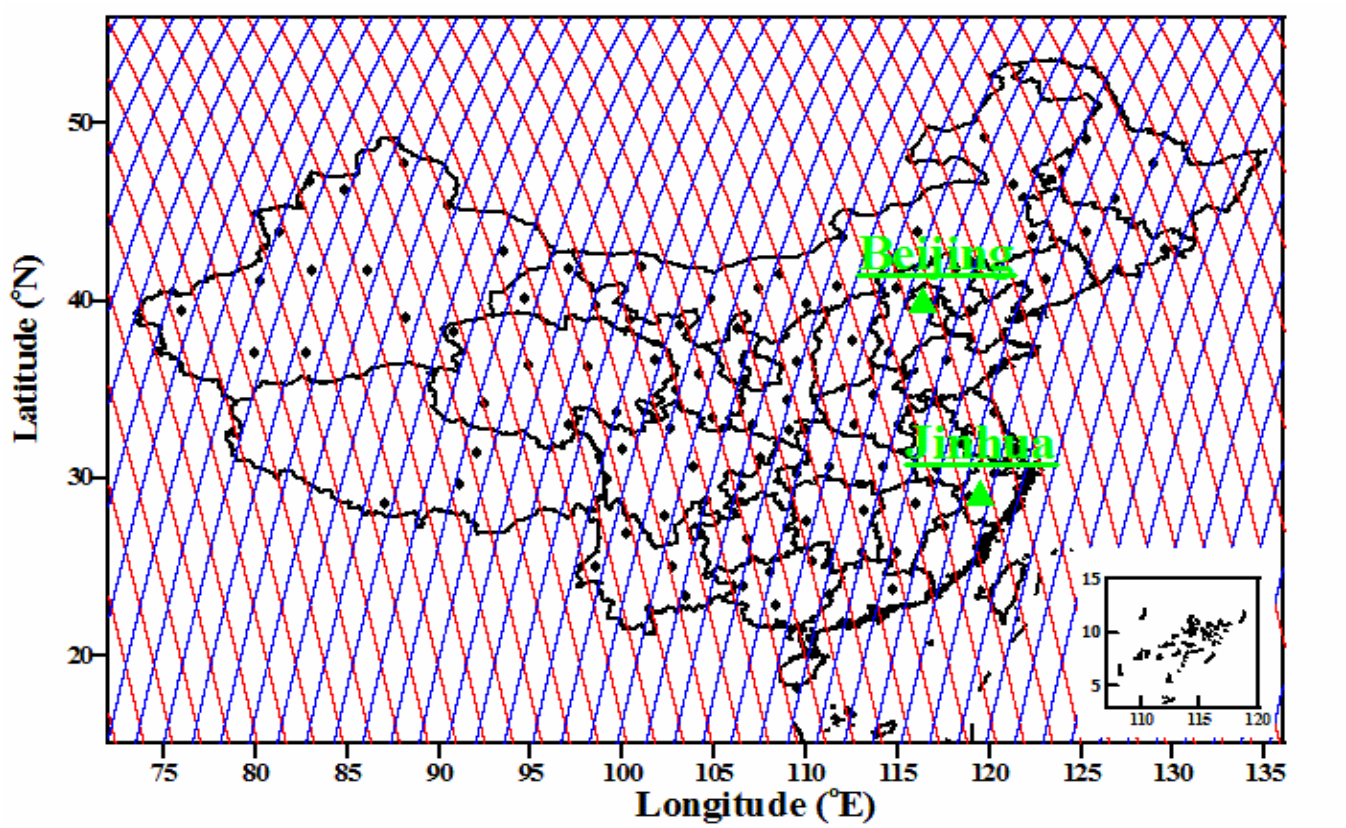

Figure 1. Geographic distribution of radiosonde sites and ground tracks for CALIPSO over China. Red lines represent the ground tracks for the CALIOP daytime orbits (in ascending mode), while blue lines for the CAILOP nighttime orbits (in descending mode). The black dots denote all radiosonde sites operated and maintained by China Meteorological Administration. Beijing and Jinhua (green solid triangles) are two sites deployed with ground-based lidar.

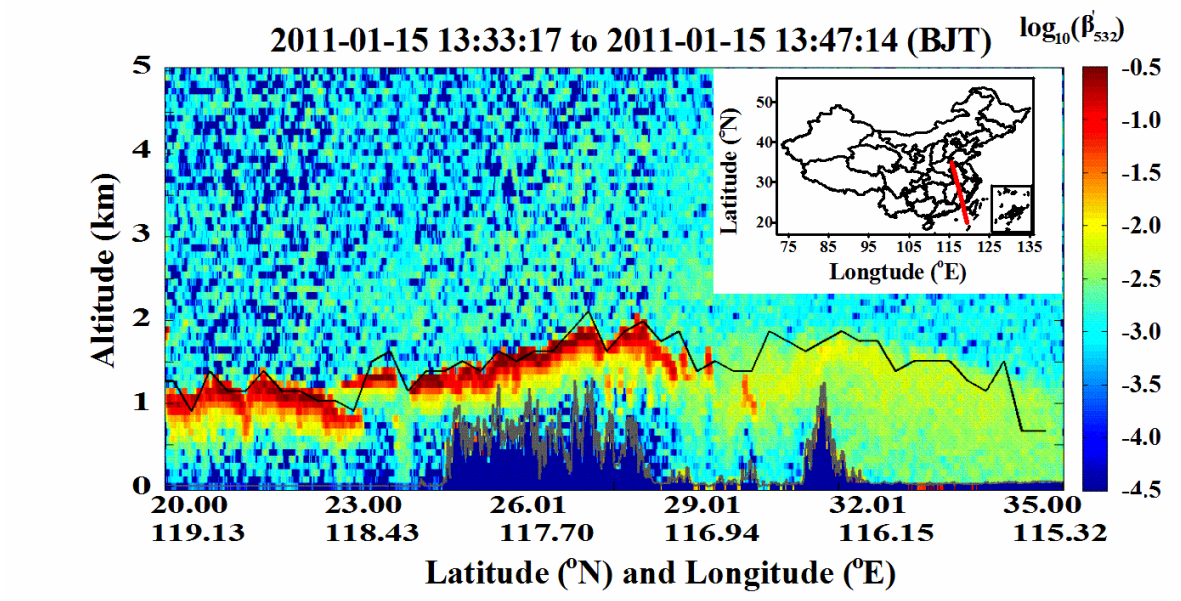

Figure 2. Curtain plot of attenuated backscatter coefficient as observed from CALIOP aboard CALIPSO on 15 January 2011. The black line indicates the derived PBLH (above ground level) and the grey line immediately on top of the blue region represents the terrain surface(directly extracted from CALIOP data). The red line in the inlet map corresponds to the ground track of CALIOP/CALIPSO over southeastern China.

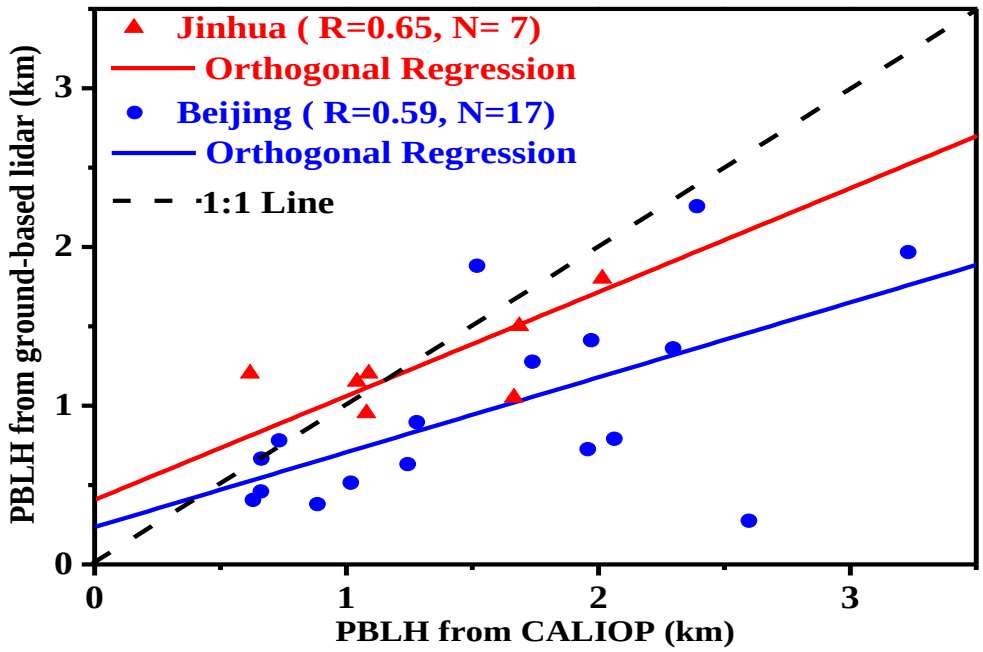

Figure 3. Scatter plot for comparing PBLHs from CALIOP to those from ground-based lidars at Beijing (blue dots) during the period January 1, 2014 to December 31, 2014 and Jinhua (red triangles) during the period of June 1, 2013 to December 31, 2013. Blue and red lines denote the linear fit to the data at Beijing and Jinhua sites, respectively, and black dash line the 1:1 correlation. The number of collocated data samples and corresponding correlation coefficient(R) are shown as well.

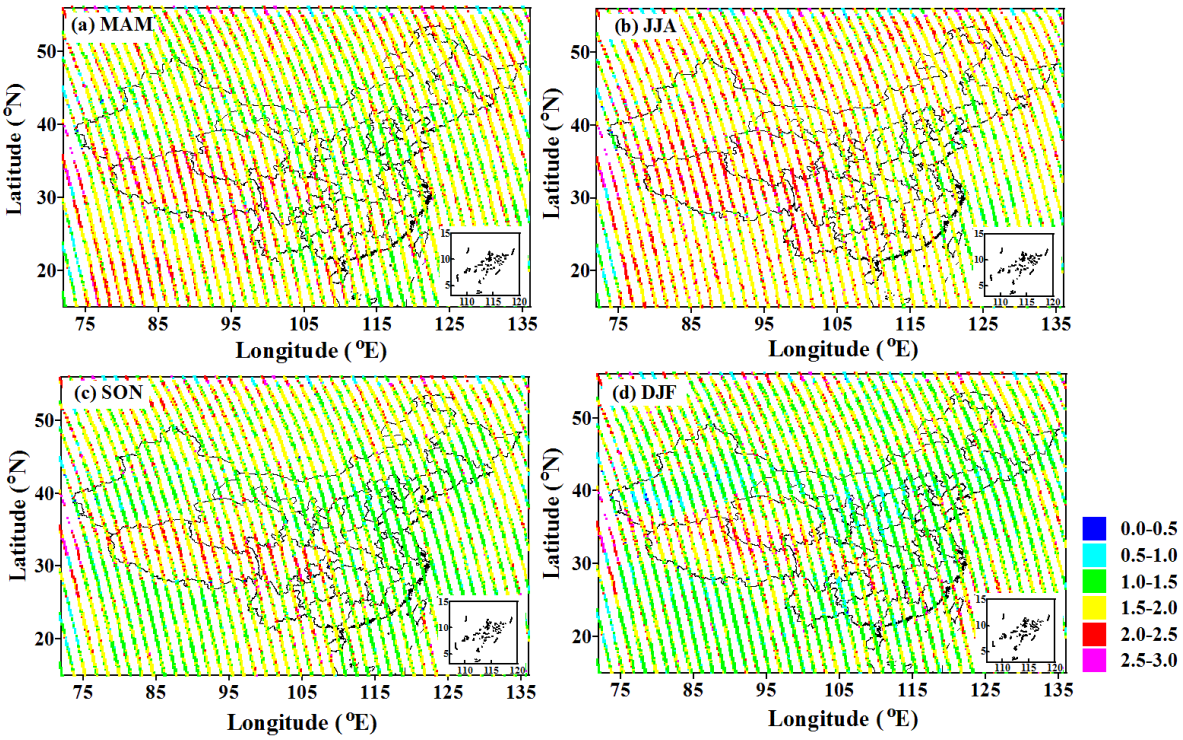

Figure 4. Spatial distributions of climatological PBLHs derived from CALIOP at 1330 BJT in (a) spring (March-April-May, MAM), (b) summer (June-July-August, JJA), (c) autumn (September-October-November, SON) and (d) winter (December-January-February, DJF) during the period 2011 - 2014. Horizontal resolution is resampled to 20 km along the ground track.

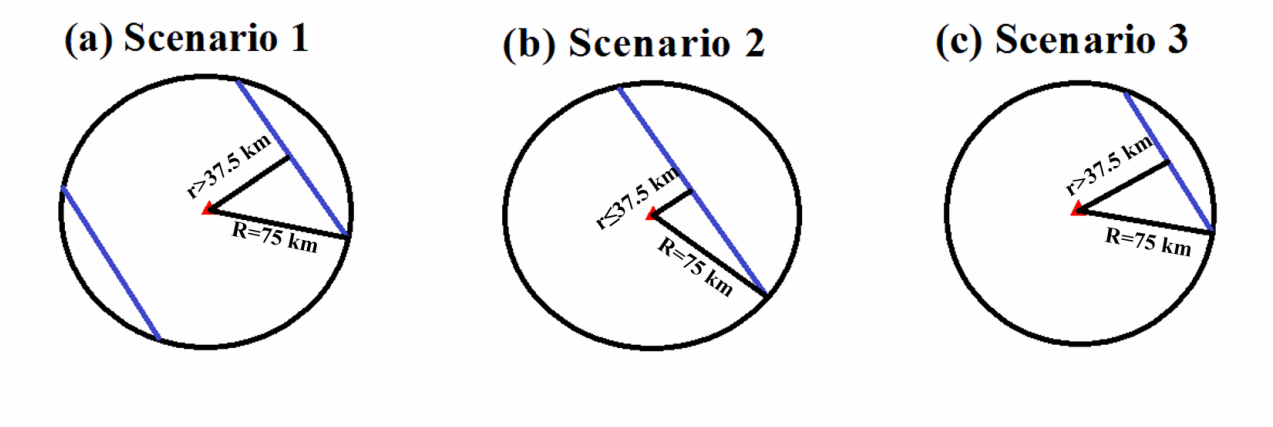

Figure 5. Schematic diagrams s showing the location of CALIOP ground tracks relative to radiosonde sites according to (a) Scenario 1 (with two CALIOP ground tracks, the shortest distance to which each is more than 37.5km from radiosonde site); (b) Scenario 2 (with one CALIOP ground track, the shortest distance to which is less than 37.5km from radiosonde site; (c) Scenario 3 (with one CALIOP ground track, the shortest distance to which is more than 37.5km from radiosonde site) showing the geometric relationship of CALIOP ground tracks relative to radiosonde sites. A circle with a radius of 75 km centered at radiosonde sites was chosen to obtain averaged PBLH from CALIOP, as compared with the measured PBLH from ground-based soundings.

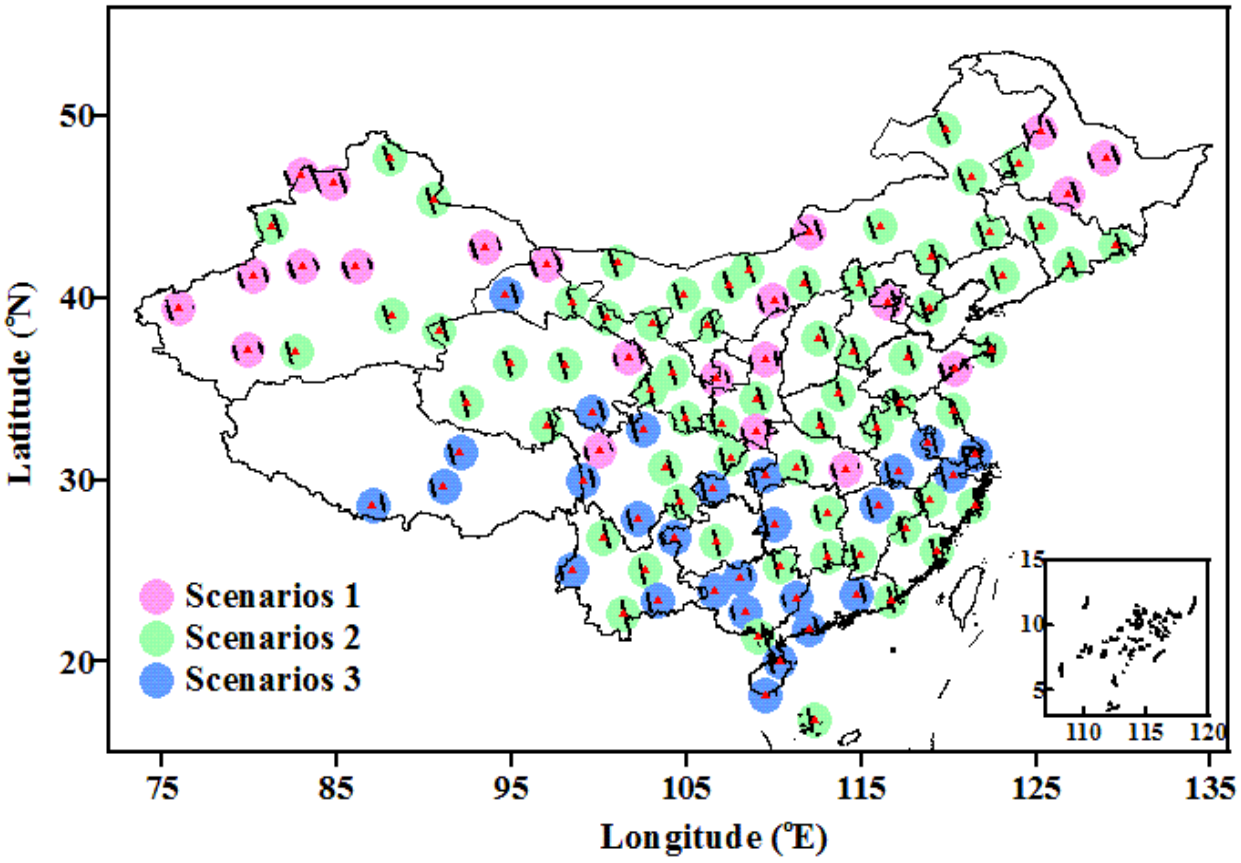

Figure 6. The geographic distribution map showing the location of radiosonde sites relative to CALIOP ground tracks over China. The red triangles denote the radiosonde sites, and the black lines show CALIOP tracks chosen for comparison analysis. The solid circles in cayon, green and blue correspond to Scenarios 1, 2, and 3 as defined in Figure 5.

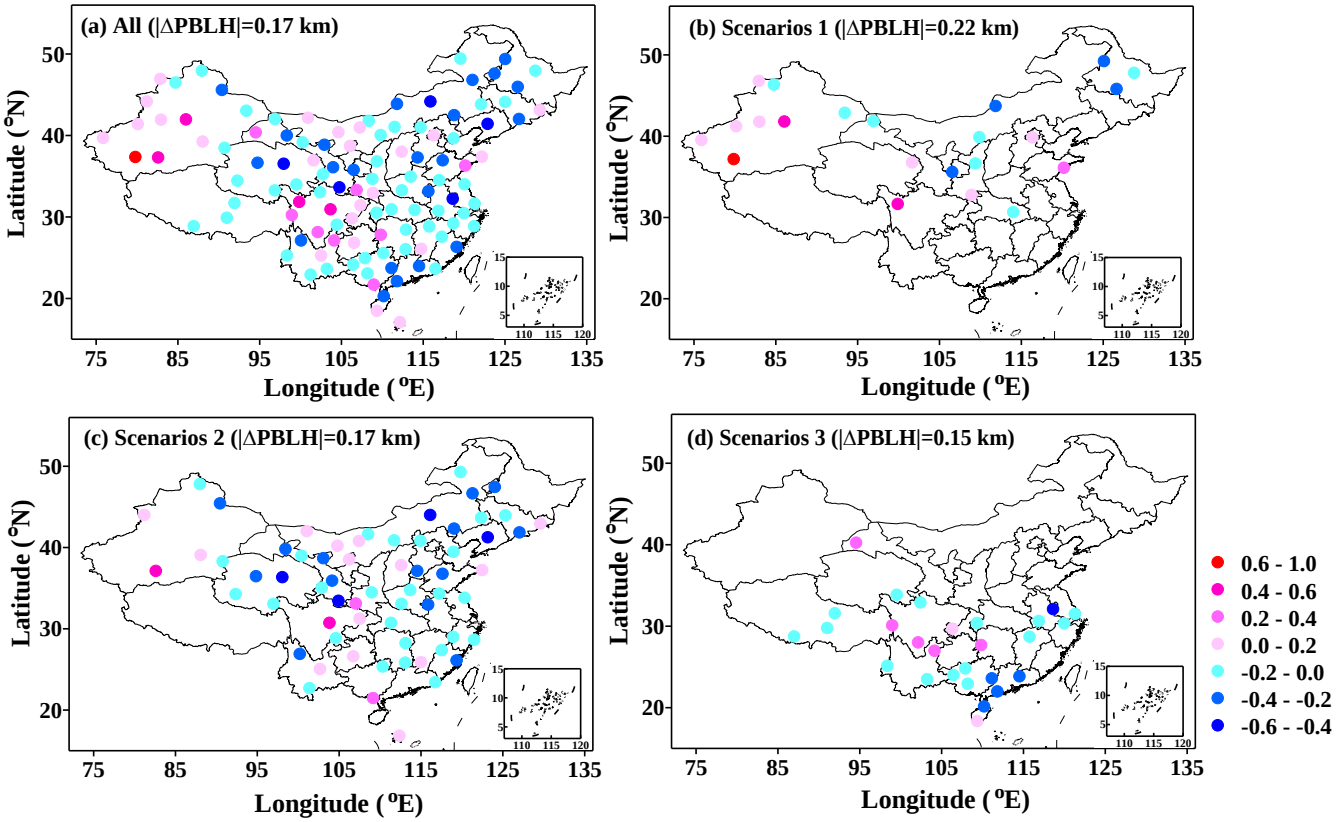

Figure 7. The geographic distribution map concerning the absolute difference of PBLH derived from CALIOP 1330 LT minus that derived from radiosonde observations at 1400 BJT in the summertime (June-July-August) during the period of 2011-2014. The differences of PBLHs are shown for all radiosonde sites in China (a), the radiosonde sites belonging to Scenario 1 (b), Scenario 2 (c), and Scenario 3 (d), respectively.

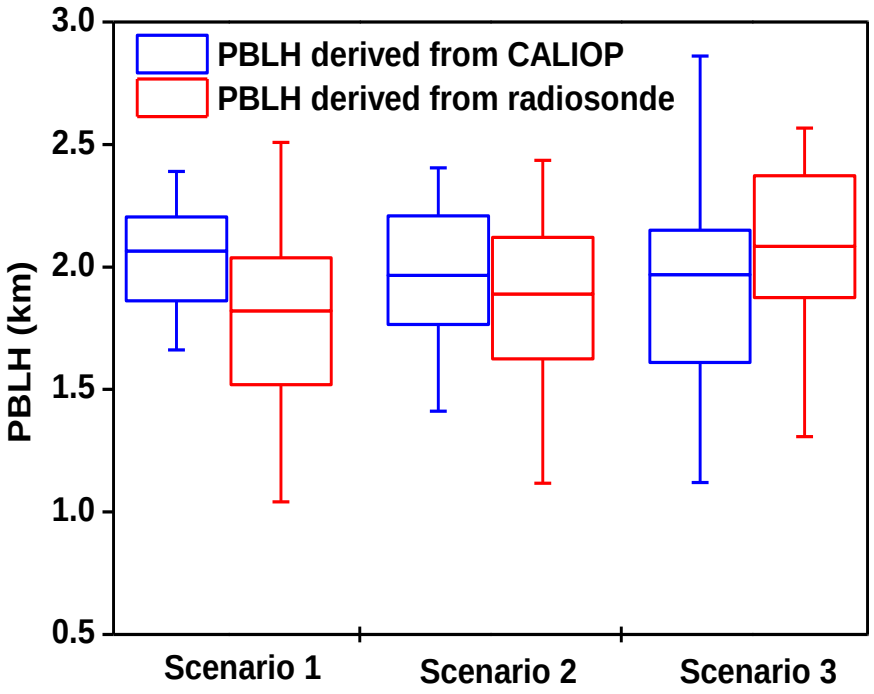

Figure 8. Box-and-whisker plot showing the 5th, 25th, 50th, 75th and 95th percentile values of PBLH derived from CALIOP (in blue) and radiosonde (in red) for each scenario. Note that only 1400 BJT radiosonde are used to make comparison with afternoon CALIOP-derived PBLHs.

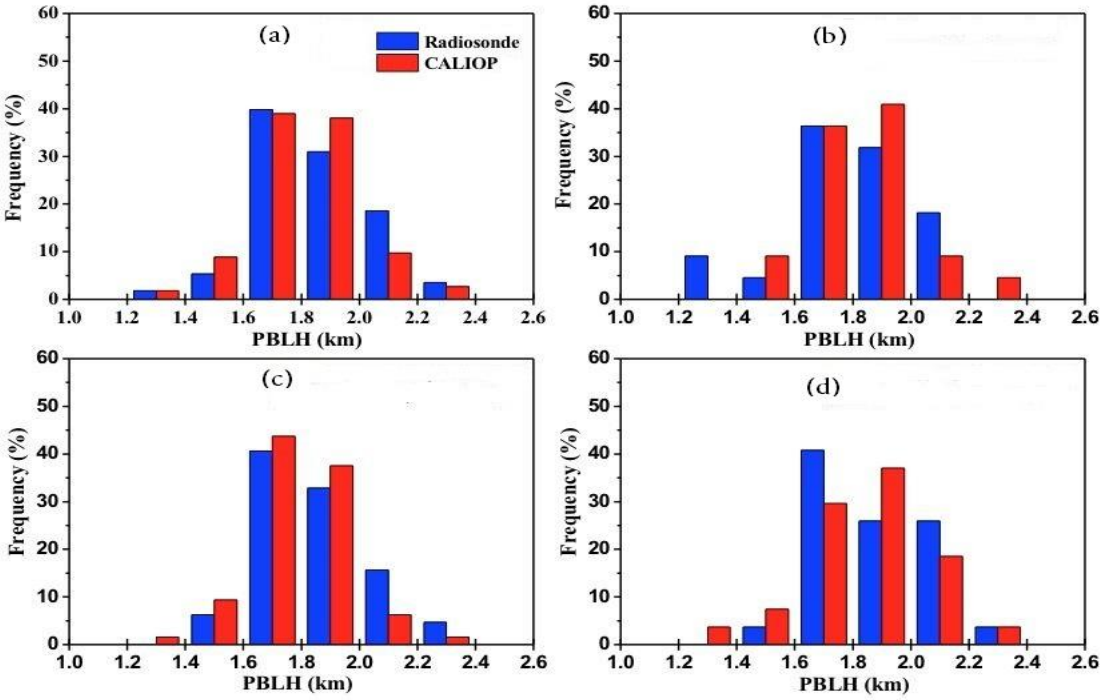

Figure 9. Histogram of the number of radiosonde sites, stratified by binned radiosonde-derived mean PBLHs (blue bars, 1400 BJT) and CALIOP-derived mean PBLHs (red bar, around 1330 LT) over China in the summertime (June-July-August) during the period of 2011-2014 for all radiosonde sites (a), the radiosonde sites belonging to Scenario 1 (b), Scenario 2 (c), and Scenario 3 (d), respectively. The frequency is calculated as the ratio of the number of radiosonde site in each PBLH bin to the total number of radiosonde sites. Note that the statistic results are only limited to the samples with collocated CALIOP- and radiosonde-derived PBLHs.